Bio-Inspired Distance Estimation using the Self-Induced Acoustic Signature of a Motor-Propeller System

Luke Calkins, Joseph Lingevitch, Loy McGuire, Jason Geder, Matthew Kelly,
Michael M. Zavlanos, Donald Sofge & Daniel M. Lofaro

***Abstract*—In this paper we propose an algorithm to actively control the distance of a motor-propeller system (MPS) to a large obstacle using data from a single microphone. The method is based upon a broadband constructive/destructive interference pattern across the audible frequency band that is present when the MPS is near an obstacle. By taking the difference between the power spectrum in the obstacle-free case and the spectrum when recording near an obstacle, a broadband oscillation with respect to frequency is revealed. The frequency of this oscillation is linearly-related to the distance from the microphone to the wall. We present both static and dynamic experiments showcasing the ability of the proposed method to estimate the distance to a wall as well as actively control it.**

I. Introduction

In nature, acoustic sensing is used in many tasks including localization, collision avoidance, navigation, and hunting. Prime examples of in-air echolocation, a form of acoustic sensing using reflected sound to locate objects, can be observed in many bat species whose other senses, such as sight and smell, pale in comparison to that of their mammalian counterparts. By exploiting their unique echolocation capabilities, it has been shown that these bats are able to locate and track prey, and also acquire and internally reconstruct a high-resolution map of their surroundings for navigation. By emitting ultrasonic pulses and analyzing the return signatures, bats can identify objects in the echoes and localize themselves within their surroundings. Of the approximately 1200 known species of bats, 85% use echolocation to navigate through the environment [1].

Exploiting bio-inspired principles for optimized guidance and control (G&C) of aerial platforms has been an area of intense research for many years. Specifically, for micro air vehicles (MAVs), these research topics include studying and integrating principles of optic flow, mimicking biological olfaction systems for chemical sensing capabilities, and developing proprioceptive type sensors for autonomous flight stabilization. While these modalities have made significant gains within the MAV community, utilization of acoustic signatures for G&C has not been as widely explored. The focus of this effort is to exploit bio-inspired principles of acoustic localization, specifically using propulsion system generated noise, for improved situational awareness and G&C of MAVs.

Acoustic sensors have been integrated into robotic platforms for many different purposes. This includes using onboard microphone arrays to localize external sources as in [2], or external fixed arrays to localize a robot making noise [3]. More advanced processing has been explored such as incorporating the Doppler-shift due to MAV motion to localize narrowband sources on the ground [4].

Robotic networks have also been enhanced with the use of acoustic sensing. In [5], the authors combine ultrasonic sensing with vision to perform localization in robotic networks in the absence of GPS. Other works use arrays to localize leader MAVs in swarming behavior [6]–[8]. Aside from sensing other robots making noise, acoustics have also been used for obstacle detection in robotics applications. Ultrasonic sensors are the most popular acoustic sensor used for obstacle avoidance in robotics [9], [10]. More sophisticated acoustic sensors have also been investigated including acoustic vectors sensors in sense-and-avoid applications [11]. A review on state-of-the-art techniques regarding the utilization of acoustics for guidance and navigation of surface and aerial vehicles is given in [12].

More recently, bio-inspired approaches involving acoustics have begun to emerge for obstacle detection and navigation in robotics. One such example is given in [13] in which the authors try to mimic the behavior of bats through sonar systems on ground robots. However, these systems tend to employ many microphones and scanning sound beams in ways that are not similar to the biological solution seen in bats. Other approaches try to mimic biological systems more closely by using two microphones acting as the two ears in order to simultaneously map an environment and navigate obstacles [14], or analyze the dynamic of the bat-obstacle interaction [15]. This is more closely related to the way bats utilize echolocation. Other bio-inspired approaches perform obstacle detection based on time-of-flight [16], acoustic flow-fields [17] and Doppler-shifts [18]. In [19], bio-inspired acoustics are utilized for navigation of MAVs with fixed ultrasonic sensors mounted in the environment. Utilization of the acoustic signatures of real-world MAVs for situational awareness has not been widely explored.

In 2014, a species of bat that previously was not known to possess the biological structures in order to echolocate was shown to exhibit a crude form of echolocation using bio-sonar clicks from their wings [20]. While this primitive form of echolocation cannot be utilized for real-time obstacle avoidance of thin objects such as wires, it has been demonstrated that these fruit bats can identify and avoid collisions with large surfaces. Inspired by the results in [20], in this work we employ a strategy that leverages the self generated noise already present from motor-propeller systems (MPSs) present on MAVs. The benefits of such an approach is a lightweight, low power sensing system since MAV platforms are subject

to size, weight and power constraints and in general, fewer sensors are more desirable. Specifically, by comparing the broadband frequency spectrum between the free-field and near-an-obstacle case, an oscillatory pattern in the power spectrum with respect to frequency can be observed due to constructive/destructive interference caused by reflections from the obstacle. This oscillating frequency is linearly related to the associated time-delay for an acoustic wave traveling from the microphone to the wall and back. By extracting this time delay from the frequency domain data, we can estimate the distance to the wall. The contribution of this paper is the first demonstration of active distance control of a MPS using acoustic data under self-induced noise. Whereas existing solutions in robotics use active solutions based on ultrasonic sensors, or sonar, we take a passive lightweight approach that exploits the sound already created from a MPS. This work could be utilized as a component in a higher level task such as navigation.

The rest of this paper is organized as follows. In Section II, the obstacle distance estimation in the presence of MPS noise problem is defined and the acoustic model and proposed algorithm for distance estimation is given. Experimental results are presented in section III before concluding remarks are given in section IV.

II. Problem Definition & Methods

Consider a small motor-propeller system (MPS) near a large obstacle. Assume a microphone is placed between the MPS and the obstacle. Furthermore, assume the motor is operating at a known power level and that the only sound in the environment is due to the propeller spinning and the motor-noise. The problem we address in this paper is as follows.

Problem 2.1: Given a MPS generating noise under normal operation and a microphone placed in between the MPS and and a large obstacle, determine the distance to the obstacle and actively control it using only microphone data.

In order to solve Problem 2.1, we employ a physics-based acoustic model of a simple reflecting surface near a spherical attenuating sound source. We examine the broadband frequency response of this model in order to detect distance to obstacles. This is possible due the outgoing and reflected wave causing constructive and destructive interference at different frequencies. The use of such a model makes the approach generalizable to any given MPS.

A. White-Noise Emitter

Consider a MPS placed near a wall with a microphone placed along a straight line from the MPS to the wall. Assume this line is perpendicular to the wall. First, consider the MPS to be a white noise emitter, i.e., its frequency domain spectrum is a horizontal line. Let d_0 be the distance from the wall to the microphone and d_1 be the distance from the wall to the MPS. Assume $d_1 > d_0$, i.e. the MPS is farther away from the wall compared to the microphone. In a 3D environment, the complex frequency domain response at the microphone without the wall present is given as a $1/r$ attenuation from spherical spreading according to

$$\frac{e^{ik(d_1-d_0)}}{d_1-d_0}, \tag{1}$$

where $k = \omega/c$ is the wave number given the wave angular frequency ω and speed of sound c. Here, we have assumed the convention of the factor $e^{i\omega t}$ in the forward Fourier transform, and $e^{-i\omega t}$ in the inverse transform. With the wall present, under the assumption that the wall is a sound-hard boundary and therefore reflects all acoustic energy incident upon it, the response at the microphone can be determined by placing an image source at an equal distance of d_1 on the other side of the wall, resulting in a distance of $d_0 + d_1$ between the image source and the microphone. The response at the microphone can then be evaluated as the summation of the true source and image source as

$$\frac{e^{ik(d_1-d_0)}}{d_1-d_0} + \frac{e^{ik(d_1+d_0)}}{d_1+d_0}. \tag{2}$$

Assume that the distance from the MPS to the wall is fixed but the distance from the microphone to the wall is varied, i.e., d_1 is fixed, but d_0 varies. The broadband power spectrum in dB of Equation (2) is shown in Figure 1 for different values of d_0. Since the power spectrum in dB is defined as $10\log_{10}|X|^2$ where $|X|$ is the magnitude of the complex frequency domain signal X, the influence of d_0 and d_1 on the power spectrum can be seen by taking the complex magnitude squared of Equation (2), which after some manipulation of trigonometric identities comes out to

$$\frac{1}{(d_1-d_0)^2} + \frac{1}{(d_1+d_0)^2} + \frac{2\cos(2kd_0)}{d_1^2-d_0^2}, \tag{3}$$

which is a periodic function that oscillates at frequency $4\pi d_0/c$ with respect to the temporal frequency f in Hz as shown in Figure 1. Therefore, the oscillation with respect to frequency is a function of d_0, the distance from the microphone to the wall. The amplitude of the oscillation depends on the difference between d_1 and d_0. Therefore, the distance to the wall can be estimated by determining the frequency of oscillation of the microphone spectrum. Note that similar expressions for the case where $d_0 > d_1$ can be derived in which case, the direct path distance would be $d_0 - d_1$ and the reflected path distance would be $2d_1 + (d_0 - d_1) = d_0 + d_1$. However, as discussed in Section III, the interference effects for this configuration were not observed in experiment.

The use of white-noise emitters here serves in illustrating the interference effects in the frequency domain. In reality, the MPS spectrum is not white, but rather has peaks at specific frequencies corresponding to the blade passing frequency and associated harmonics as well as the noise from the motor.

B. Non-White Emitter

Now, consider the frequency response at the microphone due to an non-white noise MPS. Denote the direct wave

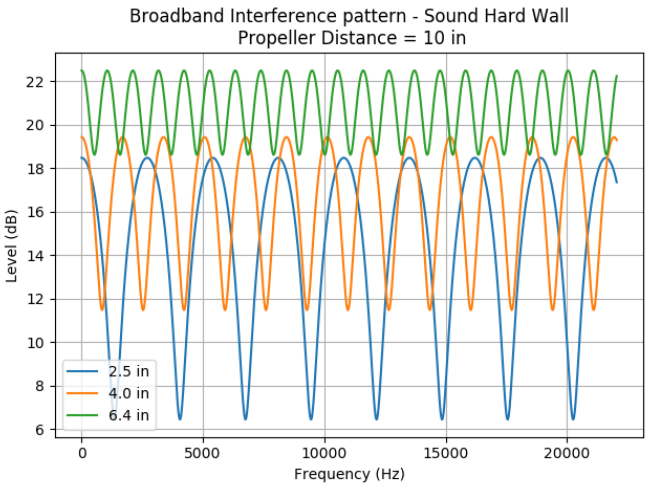

Fig. 1: Broadband interference pattern in dB (reference = 1)

frequency response as $\hat{p}_d(\omega)$, which now has a frequency-dependent magnitude. The measured response in the frequency domain at the microphone $\hat{p}_m(\omega)$ is then given as

$$\hat{p}_m(\omega) = \hat{p}_d(\omega) + a_r \hat{p}_d(\omega) e^{i\omega\tau}, \tag{4}$$

where the complex coefficient a_r incorporates spreading and reflection losses as well as a phase shift ϕ. The exponential term is a time-delay $\tau = 2d_0/c$ relative to the direct arrival where c is the speed of sound. The power spectrum at the microphone $\hat{p}_m(\omega)$ is thus the product of the direct-wave power spectrum and the oscillatory interference pattern due to the reflection

$$|\hat{p}_m(\omega)|^2 = |\hat{p}_d(\omega)|^2(1 + a_r^2 + \cos(\omega\tau + \phi)). \tag{5}$$

From equation (5), it can be seen that the microphone sees the product of the non-flat source spectrum and an interference term and therefore the frequency of oscillation τ cannot be easily extracted. However, if the direct-wave spectrum is known, then dividing (5) by $\hat{p}_d$, where the dependence on ω is dropped for brevity, we are left with

$$\frac{|\hat{p}_m|^2}{|\hat{p}_d|^2} = 1 + a_r^2 + \cos(\omega\tau + \phi). \tag{6}$$

For a given MPS, the free-field power spectrum is a function of the propeller properties, the motor, and the controls to the motor. Given a specific motor and propeller, the power spectrum depends on the pulse-width modulation (PWM) signal sent to the motor which is defined by a frequency and duty-cycle. For the work presented in this paper, we assume the PWM frequency f_{pwm} is held fixed, and the power to the motor thus depends on the duty cycle d_{pwm} $(0-1)$ supplied to the motor.

The free-field response of the MPS can be measured and stored ahead of time for different values of d_{pwm} while keeping f_{pwm} constant. Then, given the current operating d_{pwm}, the power spectrum ratio (6) can be evaluated and the interference pattern revealed. Since power spectra are often examined in dB, instead of computing $|\hat{p}_m|^2$ / $|\hat{p}_d|^2$, we look at $10\log_{10}(|\hat{p}_m|^2 \text{ / } |\hat{p}_d|^2) = 10\log_{10}(|\hat{p}_m|^2) - 10\log_{10}(|\hat{p}_d|^2)$. We refer to this as the dB level difference

$$L_\Delta = 10\log_{10}(|\hat{p}_m|^2) - 10\log_{10}(|\hat{p}_d|^2). \tag{7}$$

After computing (7), frequency analysis on L_Δ must be conducted to extract τ. Specifically, by taking the fast Fourier transform (FFT) of L_Δ with the ω variable acting as the "time" variable and τ as the "frequency" to be extracted. The bin corresponding to the maximum peak of the corresponding spectrum is taken as the estimate for τ where each bin corresponds to a specific value of τ. The distance estimate can then be evaluated as $d_0 = c\tau/2$ where the factor of 2 is needed since the delay represents the time for the wave to travel from the microphone to the wall and back. The details of estimating the microphone distance to the wall using time-averaged spectra are shown in Algorithm 1.

Algorithm 1 Time-averaged Distance Estimation

Require: Motor PWM duty cycle d_{pwm}
Require: Motor PWM freuquency f_{pwm}
Require: Free-field spectra in dB $\hat{p}_d(d_{pwm}, f_{pwm})$
1: Compute FFT of microphone stream $\hat{p}_m$
2: Compute dB level difference $L_\Delta = \hat{p}_m - \hat{p}_d$
3: Compute FFT of the L_Δ, call it FFT_Δ
4: Find time delay as $\Delta t = argmax(FFT_\Delta)$
5: Compute distance $d_0 = c\Delta t/2$

III. Experimental Results

In this section, we present results from a static distance estimation experiment as well as an active control experiment servoing a motor-propeller system (MPS) to a wall.

A. Static Distance Estimation

We present the results of a static experiment in which 8 microphones are placed in between a 3-bladed propeller controlled by an 8 mm brushed DC motor. All processing is done for a single microphone, but 8 were set up to illustrate the ability to detect different distances accurately. The motor is fastened to a 3D printed structure and connected to a constant 3.7 V power supply. The power to the motor is controlled via pulse width modulation (PWM), which is defined by a frequency f_{pwm} and duty cycle d_{pwm}. The PWM signal is generated by a Teensy 3.2 micro-controller and output at 44.1 kHz. The acoustic data acquisition system is a small Linux computer equipped with a 8-channel Advantech PCIE1802 24-bit A/D card at 44.1 kHz sample rate. The microphones are 0.25 inch PCB Model 130F22 ICP electret array microphones. The experimental setup can be seen in Figure 2.

Data was collected with a constant PWM rate of $f_{pwm} = 5$ kHz and duty cycle $d_{pwm} = 50\%$, i.e. a 5 kHz square wave. First, data was recorded for 30 seconds and the power spectral density was computed by splitting up the data into 1024 point samples using a 50% overlap. The spectra are averaged over 30 seconds at constant d_{pwm} and f_{pwm} for both the free-field and

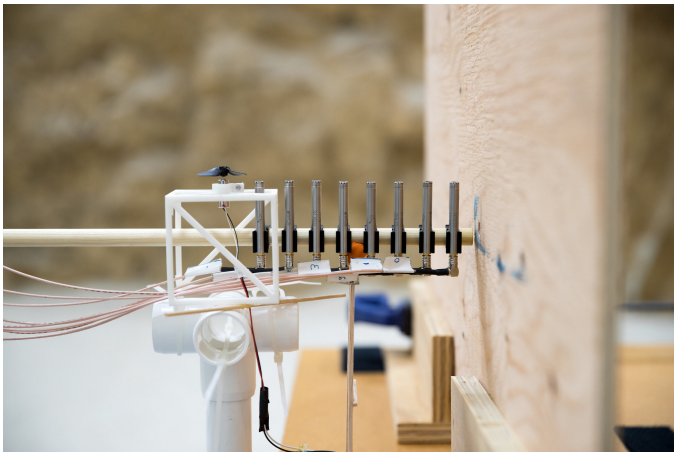

Fig. 2: Static experimental setup for wall distance detection

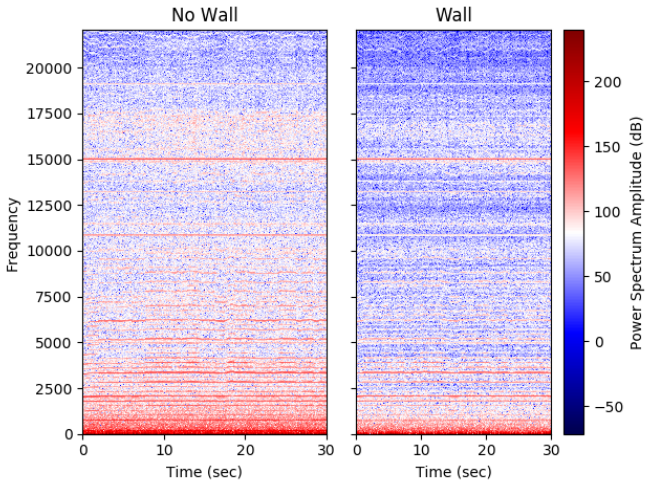

Fig. 3: No wall (free-field) vs wall present spectogram

wall present cases and then the analysis for distance estimation is a post processing step. A spectogram is shown in Figure 3 both without the wall present and with the wall positioned 0.105 meters away from the microphone. A prominent peak can be seen at 15 kHz which is the first harmonic of a 5 kHz square wave. The result of taking the difference between the wall and no-wall spectrum is shown in Figure 4. A noticeable oscillation with respect to frequency can be seen as faint horizontal lines. By applying Algorithm 1 to the time-averaged spectra of each microphone channel, the distance from each microphone to the wall can be estimated. Results are shown in Figures 5 - 7. The oscillation is not detectable on microphones 6 and 7, the two closest microphones to the MPS. This is due to the sound very close to the propeller being much higher in level as compared to the reflected waves, as well as near field effects not captured by the model. Experiments were also conducted in which the microphones were placed on the other side of the MPS relative to the wall, i.e. $d_0 > d_1$ as explained in Section II-A. The interference pattern was not observable in this case likely for similar reasons.

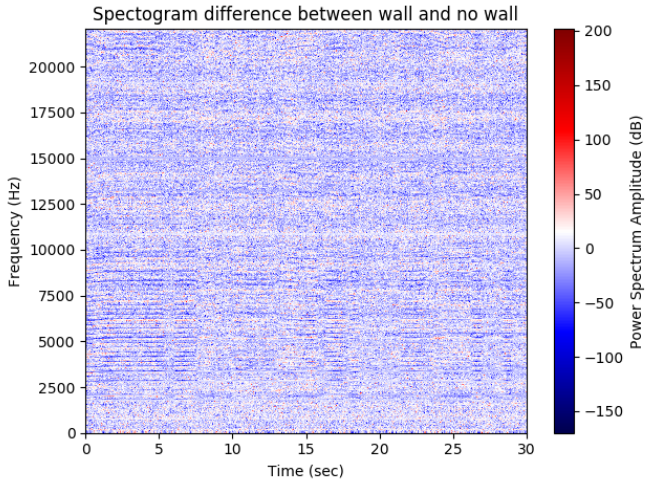

Fig. 4: Spectogram of dB difference between wall and no wall present cases.

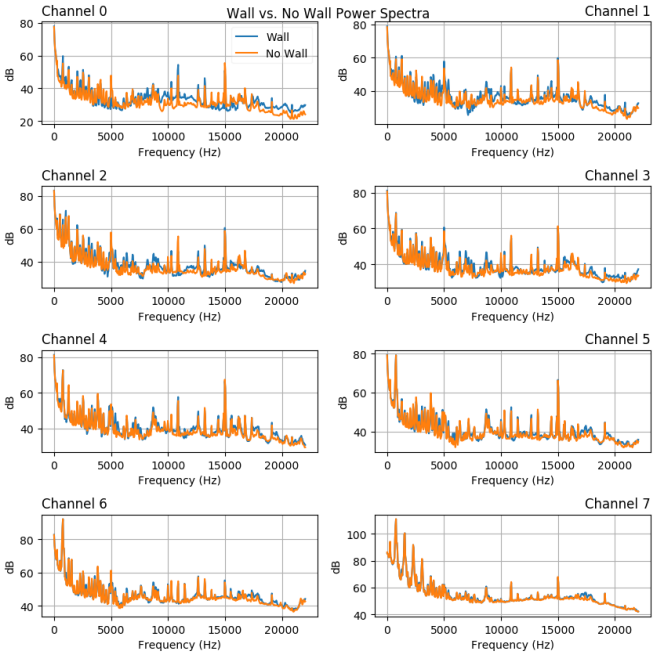

Fig. 5: Power spectra of with and without the wall present for all 8 channels

B. Active Servo Experiment

In this section we present results for an experiment where we actively control the distance of a MPS to a wall. This experiment demonstrates the feasibility of the proposed method being used in real-time for control purposes and for being implemented on a micro air vehicle for obstacle detection in future work. A MPS is mounted on a horizontal arm which is fixed at one end but free to rotate about the fixed end. A wheel is placed on the bottom of the arm such that the arm can rotate laterally toward and away from a fixed plywood wall. An 8.5 mm brushed motor with a 2-bladed propeller is mounted in the middle of the pivoting arm and acts as the sound source. An Adafruit MEMS pulse density modulated (PDM) microphone

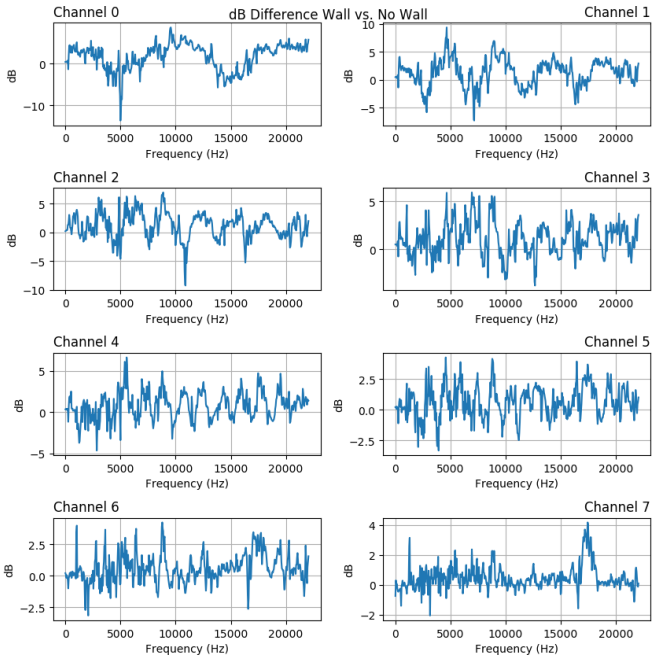

Fig. 6: dB level difference between the wall and no wall power spectra as seen in Figure 5 for all 8 channels. The dominant oscillating frequency can be seen to increase as the distance from the wall increases.

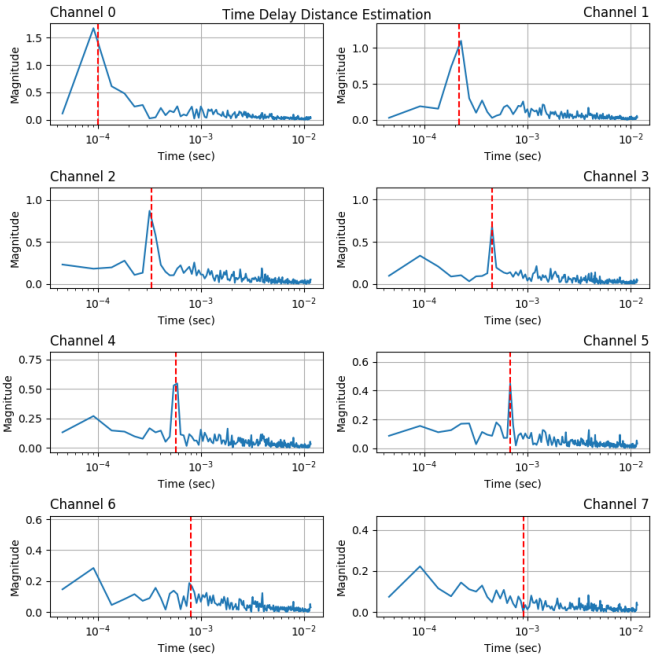

Fig. 7: Time delay approximation taken as the maximum peak in the FFT of the dB level difference curves in Figure 6 for all 8 channels. Red vertical line represents expected delay based on microphone's distance from the wall.

Algorithm 2 Active Distance Control Algorithm

Require: free-field spectra table $\hat{p}_d$ (100×256)
Require: Distance servo setpoint d_{ref}
Require: Proportional gain K_p
Require: Constant operating PWM frequency f_{pwm}
while true **do**
  Get current operating duty cycle d_{pwm}
  Get associated free-field spectra $\hat{p}_d(d_{pwm}, f_{pwm})$
  Compute FFT of microphone stream $\hat{p}_m$
  Compute dB difference $L_\Delta = \hat{p}_m - \hat{p}_d$
  Compute FFT of dB level difference, FFT_Δ
  Find time delay as maximum peak $\Delta t = \text{argmax}(FFT_\Delta)$
  Compute distance $d = c\Delta t/2$
  Calculate error, $err = d_{ref} - d$
  Calculate control value $val = K_p * err$
  Set motor duty cycle to val $(-1$ to $1)$
end while

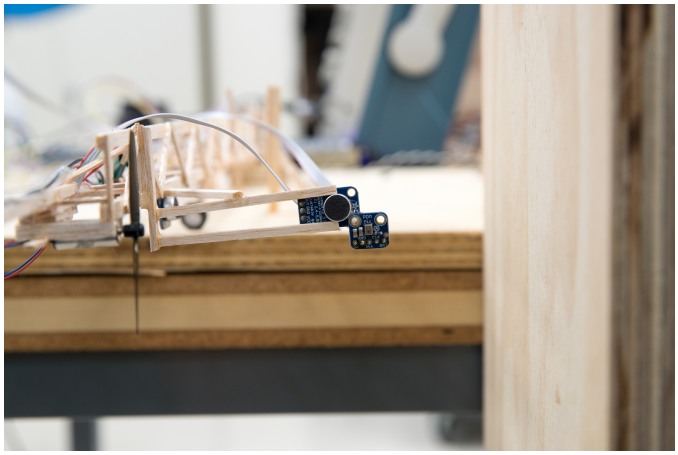

Fig. 8: MPS servo experiment. Propeller spinning at constant speed. PDM microhpone placed in between MPS and wall

is placed in between the MPS and the wall and acts as the feedback signal using the sound generated from the MPS to estimate the distance to the wall. See Figure 8. On the tip of the rotating arm, a second MPS is placed that acts as the actuation to move the arm back and forth to control the distance of the microphone to the wall. See Figure 9 for the full experimental setup. Note in Figure 9 that the microphone is not on a line perpendicular to the wall but at a slight angle.

The signal from the microphone is sampled at 44.1 kHz by the Teensy 3.2 micro-controller. As in the static experiment, the free-field spectrum is first measured for different duty cycles, while holding f_{pwm} constant at 5 kHz. A total of 100 different free-field spectra at duty cycles $0.01 - 1.0$ in increments of 0.01 were obtained. The power spectra are computed via a 1024 point fast Fourier transform (FFT), i.e., over a period of $\approx$ 23.2 milliseconds of the audio stream. Based on the current operating duty cycle, the correct free-field spectrum is retrieved, and the dB level difference is calculated according to equation (7). The result is fed into a 256 point FFT algorithm, all of the computation occurring on the Teensy micro-controller. The maximum peak (in seconds) of $FFT_\Delta = FFT(L_\Delta)$ is then extracted and the corresponding distance is calculated. This distance estimate is then compared to a distance setpoint and an appropriate command is sent to

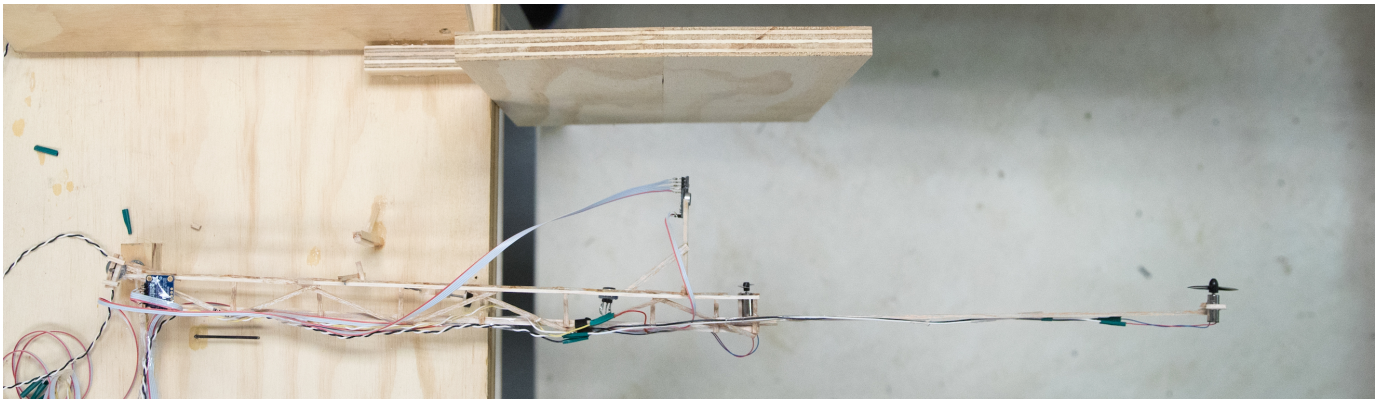

Fig. 9: MPS servo experiment. Second propeller on the far right side of the arm acts as the actuation to move the arm.

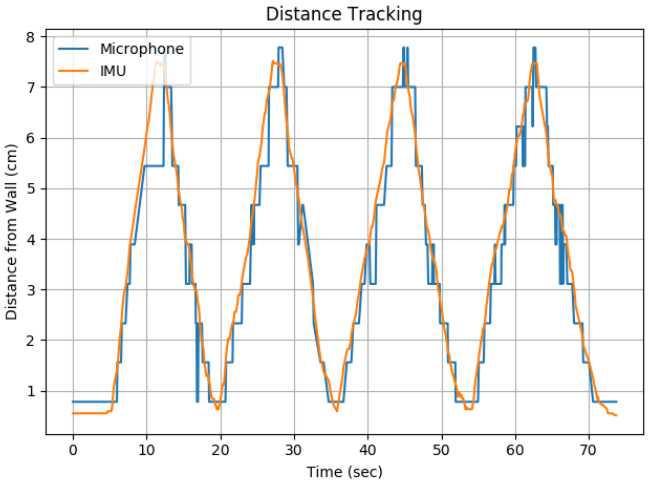

Fig. 10: Distance from wall tracking from Algorithm 2 compared to ground truth from IMU mounted on rotating arm.

the actuating MPS to reduce the error between the current and desired distance. In this paper, a simple proportional controller is used to servo the MPS. The details of the proposed method are described in Algorithm 2.

First, we present results of manually moving the arm and the output distance from Algorithm 2 tracking the ground truth distance as given by an IMU mounted at the base of the arm. The MPS was set to operate at $d_{pwm} = 0.5$, $f_{pwm} = 5$kHz, and the arm was manually moved away from the wall and back toward it 4 times and the tracking results are displayed in Figure 10. Notice that the distance estimates form a discrete set of measurements because the τ estimate is obtained from a discrete number of bins from the FFT. This causes the step like appearance of the distance output in Figure 10. A video of the system controlling the distance and reacting to perturbations away from the setpoint is given in [21] under the same MPS operating conditions.

C. Distance Detection Resolution

Here, we present analysis on the resolution of the distance estimation capability given the hardware utilized in the experiment. As the distance from the wall increases, the overall frequency of the interference pattern also increases. However, due to the size of the FFT (number of samples) being used, there is a maximum allowable detectable distance. Since the first FFT uses 1024 points and 44.1 kHz sampling rate, due to the Nyquist sampling theorem, the maximum detectable frequency is 22.05 kHz at a resolution of $44100/1024 \approx 43$ Hz. However, instead of reading all 512 bins, it is down sampled to 256 by taking every other sample in the output FFT such that it can be fed into the FFT implementation available on the micro-controller which requires either 1024 or 256 samples. Since we have 256 samples, our frequency resolution is ≈ 86 Hz. Therefore our effective sampling rate of the dB level difference curve is $1/86 \approx 0.0116$ Hz. Due to Nyquist sampling theorem, we can only detect up to half that in the FFT or 0.0058 seconds. Since the calculated time-delay represents the time for a wave to travel from the microphone to the wall and back, then the wave travels from the microphone to the wall in half that amount of time, or 0.0029 seconds which corresponds to a distance of $343 * 0.0029 \approx 1$ meter, which is the maximum detectable distance with the hardware used. Since there are 125 points from 0 to 0.0058 this gives a time resolution of $0.0058/125 \approx 4.64 \times 10^{-5}$ seconds. This corresponds to a distance resolution of ≈ 7.8 mm or ≈ 0.31 inches. This means that there are only discrete distances available in increments of 7.8 mm and the control to the motor will not be updated unless the distance changes by this incremental value.

IV. Conclusion

In this paper, we presented a method to estimate and control the distance of a motor-propeller system (MPS) to a large obstacle using only acoustic data from a single microphone in the presence of sound created by the normal operation of the MPS. By knowing the free-field frequency-domain acoustic response of the MPS under different operating conditions, we were able to actively servo its position relative to a large obstacle by performing real-time spectral analysis. Future work includes robustness studies under different operating conditions, combining information from multiple microphones, as well as a navigation experiment with a micro aerial vehicle.

REFERENCES

[1] M. Knörnschild, K. Jung, M. Nagy, M. Metz, and E. Kalko, "Bat echolocation calls facilitate social communication," *Proceedings of the Royal Society B: Biological Sciences*, vol. 279, no. 1748, pp. 4827–4835, 2012.

[2] S. Ogiso, T. Kawagishi, K. Mizutani, N. Wakatsuki, and K. Zempo, "Self-localization method for mobile robot using acoustic beacons," *ROBOMECH Journal*, vol. 2, no. 1, p. 12, 2015.

[3] Q. H. Wang, T. Ivanov, and P. Aarabi, "Acoustic robot navigation using distributed microphone arrays," *Information Fusion*, vol. 5, no. 2, pp. 131–140, 2004.

[4] M. Basiri, F. Schill, P. U. Lima, and D. Floreano, "Robust acoustic source localization of emergency signals from micro air vehicles," in *2012 IEEE/RSJ International Conference on Intelligent Robots and Systems*, pp. 4737–4742, IEEE, 2012.

[5] O. De Silva, G. K. Mann, and R. G. Gosine, "An ultrasonic and vision-based relative positioning sensor for multirobot localization," *IEEE Sensors Journal*, vol. 15, no. 3, pp. 1716–1726, 2014.

[6] M. Basiri, F. Schill, D. Floreano, and P. U. Lima, "Audio-based localization for swarms of micro air vehicles," in *2014 IEEE international conference on robotics and automation (ICRA)*, pp. 4729–4734, IEEE, 2014.

[7] M. Basiri, F. Schill, P. Lima, and D. Floreano, "On-board relative bearing estimation for teams of drones using sound," *IEEE Robotics and Automation Letters*, vol. 1, no. 2, pp. 820–827, 2016.

[8] J. Müller, A. V. Ruiz, and I. Wieser, "Safe & sound: A robust collision avoidance layer for aerial robots based on acoustic sensors," in *2014 IEEE/ION Position, Location and Navigation Symposium-PLANS 2014*, pp. 1197–1202, IEEE, 2014.

[9] S. Walter, "The sonar ring: Obstacle detection for a mobile robot," in *Proceedings. 1987 IEEE International Conference on Robotics and Automation*, vol. 4, pp. 1574–1579, IEEE, 1987.

[10] J. Borenstein and Y. Koren, "Obstacle avoidance with ultrasonic sensors," *IEEE Journal on Robotics and Automation*, vol. 4, no. 2, pp. 213–218, 1988.

[11] H.-E. De Bree and G. De Croon, "Acoustic vector sensors on small unmanned air vehicles," in *the SMi Unmanned Aircraft Systems*, 2011.

[12] R. Kapoor, S. Ramasamy, A. Gardi, R. Schyndel, and R. Sabatini, "Acoustic sensors for air and surface navigation applications," *Sensors*, vol. 18, no. 2, p. 499, 2018.

[13] J. M. Carmena and J. C. Hallam, "Doppler-based motion controller for an echolocating mobile robot," *Towards Intelligent Mobile Robots. Technical Report Series, Department of Computer Science, Manchester University*, 2001.

[14] I. Eliakim, Z. Cohen, G. Kosa, and Y. Yovel, "A fully autonomous terrestrial bat-like acoustic robot," *PLoS computational biology*, vol. 14, no. 9, p. e1006406, 2018.

[15] D. Vanderelst, M. W. Holderied, and H. Peremans, "Sensorimotor model of obstacle avoidance in echolocating bats," *PLoS computational biology*, vol. 11, no. 10, p. e1004484, 2015.

[16] B. Barshan and R. Kuc, "A bat-like sonar system for obstacle localization," *IEEE Transactions on systems, man, and cybernetics*, vol. 22, no. 4, pp. 636–646, 1992.

[17] H. Peremans and J. Steckel, "Acoustic flow for robot motion control," in *2014 IEEE International Conference on Robotics and Automation (ICRA)*, pp. 316–321, IEEE, 2014.

[18] J. M. Carmena and J. C. Hallam, "The use of doppler in sonar-based mobile robot navigation: inspirations from biology," *Information Sciences*, vol. 161, no. 1-2, pp. 71–94, 2004.

[19] R. Kapoor, S. Ramasamy, A. Gardi, and R. Sabatini, "A bio-inspired acoustic sensor system for uas navigation and tracking," in *2017 IEEE/AIAA 36th Digital Avionics Systems Conference (DASC)*, pp. 1–7, IEEE, 2017.

[20] A. Boonman, S. Bumrungsri, and Y. Yovel, "Nonecholocating fruit bats produce biosonar clicks with their wings," *Current Biology*, vol. 24, no. 24, pp. 2962–2967, 2014.

[21] Video clip: https://vimeo.com/360162240.